Swift Heavy Ion Irradiation of Polyaniline-Graphene Nanocomposite Films: Structural and Optical Properties

D.C. Chilukusha[1,2*], J.J. Mboukam[1,3], V.M. Maphiri[4], N. Manyala[4], M. Msimanga[1,3],

[1] PV NanoComposites R&D Platform, Department of Physics, Tshwane University of Technology, P Bag X680, 0001, Pretoria, South Africa.

[2] Department of Physics, Mulungushi University, Kabwe, 10101, Zambia.

[3]NRF iThemba LABS TAMS, Private Bag 11, WITS 2050, Johannesburg, South Africa.

[4]Department of Physics, University of Pretoria, Pretoria 0002, South Africa.

Abstract

In this study, we investigate the use of swift heavy ions to modify the structural and optical properties of PANI-graphene nanocomposite (PANI-G NC) films. PANI-G NC films were synthesized on Indium Tin Oxide (ITO)-coated glass by electrochemical polymerization of aniline in the presence of CVD-grown graphene. The films were then irradiated with 36 MeV Cu^{8+} ions at fluences between 5.4×10^{12} and 6.4×10^{13} ions/cm^2. SEM results show that irradiation up to 1.6×10^{13} ions/cm^2 leads to the formation of a porous interconnected network, with graphene nanoparticles adhering to the PANI matrix. Beyond this fluence, a dense and compact granular structure appears. Raman spectroscopy reveals enhanced Raman scattering of the polaronic lattice and the introduction of defects in graphene. At fluences exceeding 2.1×10^{13} ions/cm^2, the obtained spectra reveal a distinctive broad envelope centered at the D and G positions of graphene, characteristic of nanocrystalline graphite. X-ray diffraction shows an increase in both crystallinity and crystallite size of

* Corresponding author email: danielchilukusha@gmail.com (D.C. Chilukusha)

the PANI-G NC film with increasing fluence, followed by a decrease beyond a critical ion fluence. Optical modifications were characterized by a red shift in the UV-Vis spectrum with increased fluence. The optical band gap shows a decreasing trend with ion dose, attributed to the formation of carbonaceous clusters along the latent tracks of energetic ions. In short, this study demonstrates that swift heavy ion irradiation could be an effective tool for enhancing the structural and optical properties of PANI-G NC films and tailoring them for specific applications.

Keywords: Polyaniline, graphene, swift heavy ion irradiation, structural properties, optical properties, UV-Vis.

Highlights

- Polyaniline-graphene nanocomposite films are synthesized electrochemically
- Heavy ion irradiation modifies Polyaniline-graphene nanocomposite films
- Irradiation enhances polaronic structure and induces defects in graphene
- Crystallinity/crystallite size increase with irradiation up to a critical fluence
- Energy bandgap reduces with ion dose due to formation of carbonaceous clusters

Graphical abstract

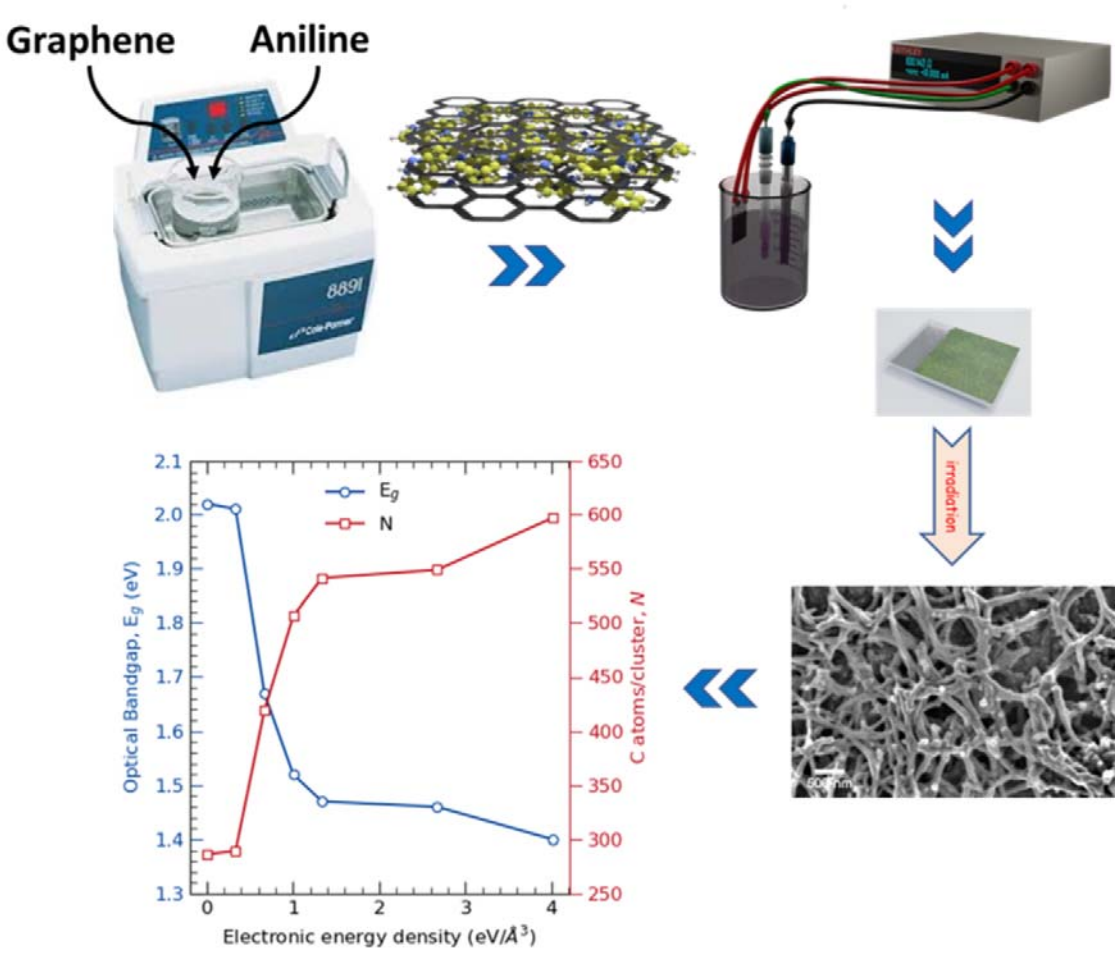

1. Introduction

In recent years, the quest for new and innovative nanomaterials has intensified as researchers aim to solve contemporary challenges in a sustainable way. Among the materials attracting attention are graphene and intrinsic conducting polymers, particularly polyaniline (PANI) [1]. Graphene, a single layer of carbon atoms densely packed in a honeycomb crystal lattice, boasts a range of extraordinary electronic, optical, magnetic, thermal, mechanical, and chemical properties that make it appealing for a variety of applications [2–4]. PANI, on the other hand, is a unique intrinsic conducting polymer with the ability to change its electrical properties by altering the oxidation state of its backbone and protonating its amine nitrogen atoms. This versatility makes it a competitive material for a number of technologies, including electronics, energy storage, and environmental protection [5,6].

The interest in PANI-graphene nanocomposites (PANI-G NCs) arises from the desire to optimize the synergies of these two materials. The van der Waals forces and π–π stacking between graphene sheets cause them to aggregate, reducing their accessible surface area and limiting their performance. Meanwhile, PANI is hindered by its poor mechanical and thermal stability, as well as structural deterioration. The introduction of graphene as a nano-filler into the PANI matrix has been shown to significantly improve its mechanical stability, while the presence of PANI nanostructures in between the graphene sheets prevents aggregation and enhances charge transport [7]. As a result, the combination of graphene and PANI not only enhances the existing properties of each material but may also introduce new, novel ones.

Swift heavy ion (SHI) irradiation, by modifying the electrical conductivity of polymeric materials, offers an alternative to traditional chemical doping of organic semiconductors [8]. This ‘doping’

method involves impinging high-energy ions onto the material's surface, inducing structural damage, and leading to changes in the material's chemical, optical, and electrical properties, depending on the specific ion species, energy, fluence, and other factors [9]. Compared to chemical doping, the key advantage of SHI irradiation is the ability to introduce well-defined. long-range structural modifications without the use of chemicals, making it an attractive option for optimizing material properties. Additionally, SHI irradiation eliminates the risk of contamination associated with chemical doping and provides greater control over the material modification process, enabling the precise tailoring of material properties [10].

SHI irradiation has been utilized for the alteration of PANI in various contexts, including pure PANI [10–15], PANI blends with other polymers [16–19], PANI composites with carbon nanotubes [20–22], and PANI doped with metals and metal complexes [17,23,24]. Other studies have also investigated the influence of energetic ion irradiation on pure graphene [25,26] as well as its composites with polymers such as PET and PMMA [27]. However, in the literature surveyed, only one report by Devi and Kumar [28] was found on the irradiation of PANI nanocomposites with graphene. The variant of graphene used in their study was reduced graphene oxide (rGO). While rGO may retain some properties of pristine graphene, the residual functional groups in the basal plane and defects introduced during the reduction process could negatively impact certain properties, such as electrical conductivity [29].

This study investigated the effects of incorporating graphene into PANI and, more importantly, the impact of SHI-irradiation on the structural and optical properties of PANI-G NC films. It was found that the properties of PANI-G NC films vary systematically with ion fluence. To the best of the knowledge of these authors, there are no reports in the literature dealing with the structural and optical properties of SHI irradiated nanocomposites of PANI and pristine graphene. The study

could provide valuable insights for the development of advanced polymeric nanomaterials with improved properties.

2. Experimental Methods

2.1. Materials

All chemicals used in this study were of analytical grade. Hydrochloric acid (32 %) was purchased from ACE Chemicals (SA) and aniline hydrochloride (99.5%) was purchased from Sigma-Aldrich (SA). Nickel foam (NF) was obtained from Alantum in Munich (Germany). The foam had a thickness of 1.6 mm and an areal density of 420 g/m^2. Indium Tin Oxide (ITO)-coated glass slides were procured from Luminescence Technology (China) and had a resistivity of 15 Ω /cm.

2.2. Synthesis of Graphene Foam

Graphene foam (GF) was synthesized using atmospheric pressure chemical vapor deposition (AP-CVD) with a polycrystalline NF template as described in Ref [30]. The NF was loaded into a quartz tube furnace and heated to 1000 ºC at a rate of ~33 ºC/min. The furnace was maintained at 1000 ºC for 15 minutes under a constant flow of argon (Ar) and hydrogen (H_2) gases at flow rates of 300 sccm and 200 sccm, respectively, to remove dissolved contaminants. Methane (CH_4) gas was then introduced into the reaction tube at 10 sccm for an additional 15 minutes, while maintaining the same temperature and flow rates of Ar and H_2 as before. The furnace was turned off and the tube moved to the cooler end to facilitate uniform deposition of graphene onto the NF. Finally, the NF was removed by etching with HCl (3.0 M) at 80 ºC, leaving behind high-quality GF. The product was washed thoroughly with deionized water to remove excess HCl and dried overnight.

2.3. Preparation of PANI-Graphene Nanocomposite Films

The PANI-G NCs films used in this study were prepared using the electrochemical cyclic voltammetry (CV) method. The electrolyte solution was composed of a 1:1 mixture of 1 M HCl

and 0.2 M aniline hydrochloride. To subsume the aniline monomers into the GF framework, the GF (1 wt.% with respect to aniline) was first pre-soaked in the electrolyte solution for 8 hours and then dispersed in this same solution by alternate sonication and stirring for 72 hours. For the preparation of the substrates, ITO-coated glass was cut into rectangular pieces of approximately 10 × 15 mm and cleaned by consecutive ultrasonication in acetone, to remove dust particles; methanol, to remove grease; acetone again, to remove methanol; and finally in deionized water, to rinse off the acetone, each solvent treatment lasting for 5 minutes. These substrates were then mounted on the working electrode of a three-electrode cell, with Ag/AgCl and platinum as the reference and counter electrodes, respectively. The submerged area of the ITO in the electrolyte was 100 mm^2 (10 mm × 10 mm), with the extremity used to maintain electrical contact with the alligator clip. Electrodeposition of the PANI-G NCs was carried out using a Keithley 2400 source-meter unit by sweeping the voltage in the range of -0.35 V to 1.7 V at a scan rate of 25 mVs^{-1} for 5 cycles. During the experiments, the source-meter was interfaced with a personal computer and monitored/controlled in real-time using version 1.5.5 of 'SweepMe!' software [31]. To provide a baseline for comparison, pure PANI samples were prepared using similar experimental conditions, but for the presence of GF.

2.4. Irradiation

Irradiation and characterization were carried out to investigate the properties of the prepared PANI-G NCs films. The irradition work was done at a 6 MV tandem accelerator using a ^{63}Cu ion beam. The films were placed inside a target chamber under high vacuum (~10^{-6} Torr) and irradiated at room temperature with a Cu^{8+} ion beam of 36 MeV energy at normal incidence. Prior to the irradiation, a Stopping and Range of Ion in Matter (SRIM) simulation was performed, using Transport of Ions in Matter (TRIM) code [32], to ascertain that Cu^{8+} ions at this energy would

traverse the entire PANI-G NC layer without being implanted. The simulation graph is appended in the supplementary information as Figure S1. From the graph, the electronic (S_e) and nuclear (S_n) energy loss values for 36 MeV Cu^{8+} ions in PANI-G films were respectively found to be 4.67 and 537 eV/Å, indicating that the passage of the ions through the film is dominated by the electronic energy loss. The films were irradiated over a 'beam-spot' area of ~ 5 mm diameter using varying ion fluences ranging from 5.4×10^{12} to 6.4×10^{13} ions/cm². To change the fluence, the irradiation time was varied while maintaining a constant beam current of 5 nA.

2.5. Characterization

The samples were characterized using a range of techniques. The morphology of the samples was observed using a Zeiss Ultra Plus 55 field emission scanning electron microscope (FE-SEM) at an accelerating voltage of 2.0 kV. The phase structure of the materials was analyzed using a Bruker BV 2D PHASER Benchtop X-ray diffraction (XRD) analyzer. The XRD measurements were taken at 2-theta values ranging from 5 to 70º, with a step size of 0.005º. The analyzer operated with a Cu $K\alpha_1$ radiation source ($\lambda = 0.15406$ nm) at 50 kV and 30 mA. Raman spectroscopy was carried out to determine the vibrational modes and was performed using a WITec alpha 300 RAS+ Confocal micro-Raman microscope with a laser wavelength of 532 nm. The spectral acquisition time was set to 15 s, and the laser power was maintained at 0.5 mW to avoid sample heating. For energy bandgap evaluation, UV-Vis spectral data were recorded using a Perkin-Elmer Lambda 365 double-beam spectrometer, fitted with double lights (deuterium and tungsten lamps). The wavelength range was set from 200 – 900 nm, with a change-over wavelength of 400 nm between the tungsten and deuterium lamps. The scan rate was set to 50 nm/min. This range of characterization techniques allowed for a comprehensive analysis of the samples, including their morphology, phase structure, and optical properties

3. Results and Discussion

3.1. SEM Results

SEM analysis was performed to investigate the morphology of PANI and PANI-G films, both with and without irradiation by SHI, to understand the effects of ion irradiation. Figure 1 shows images of unirradiated pure PANI (a) and unirradiated PANI-G composite films (b). Pure PANI shows a coarse and highly porous structure, typical of electrochemically synthesized PANI [33]. The film exhibits a morphology of agglomerated spaghetti-like nanofibers (NFs) with an average diameter of ~ 70 µm, as shown in the close-up view. In the PANI-G composites, the nanofibrous network becomes denser and more compact. Based on our results, it is difficult to clearly distinguish between the PANI and the graphene phases, probably because of their homogeneity or proximity. However, the relatively closed structure revealed in Figure 1(b1) suggests that the graphene might have filled the voids and crevices that were observed in pure PANI, resulting in a denser morphology. The presence of graphene is reported to promote the formation of agglomerate PANI NFs [34]. This enhances the stability of the composites, and combined with their porous nature, could make them potential candidates for various surface-related applications such as gas sensors and energy storage devices [35].

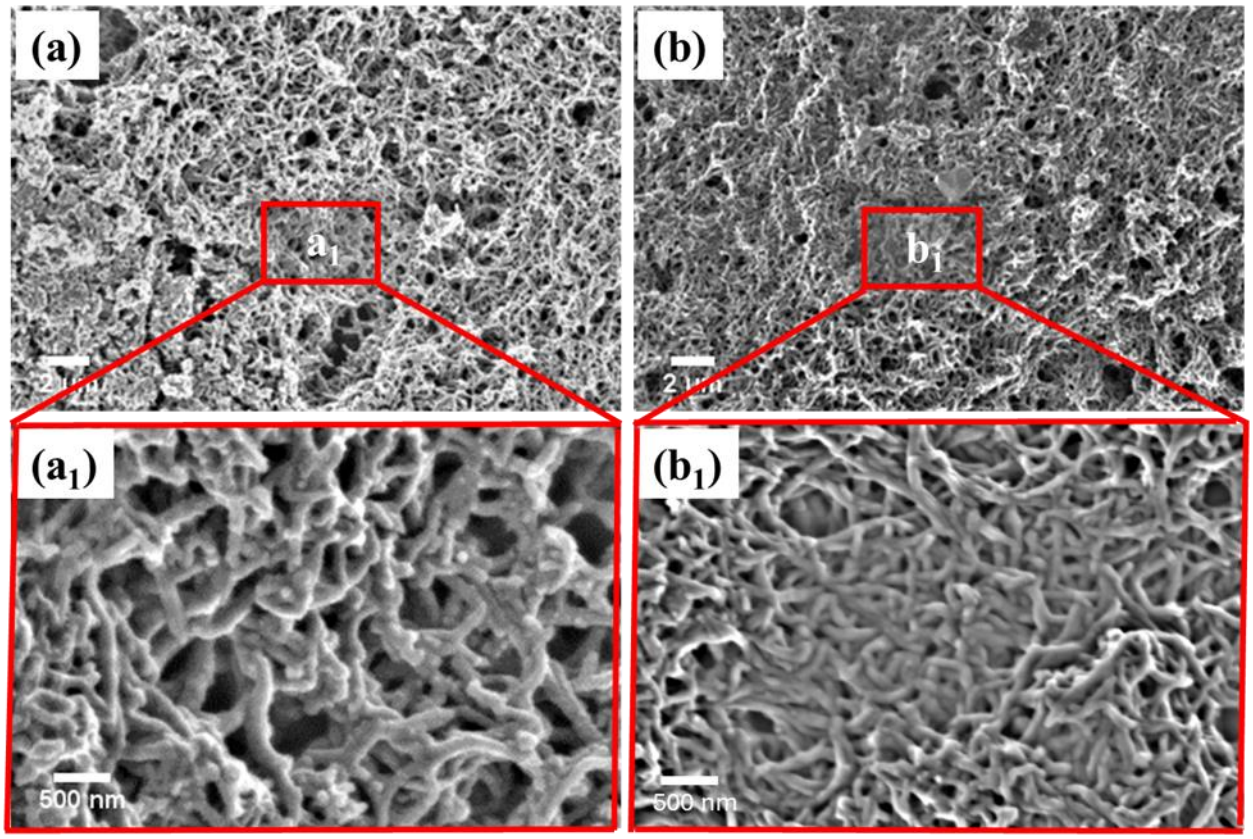

Figure 1: SEM images of a pure PANI (a) and a PANI-G NC film (b), along with up-close views of selected regions indicated by dashed rectangles (a_1) and (b_1).

SEM micrographs of PANI-G NC films irradiated at different fluences are displayed in Figure 2. The composites undergo significant changes in morphology due to SHI irradiation. As shown in Figure 2(a) – (c), there is fragmentation of the NFs leading to a more porous and less dense interconnected network. This is similar to the fragmentation of PANI nanotube observed by Devi et al [28] and is attributed to polymer chain scissoring caused by the large electronic energy deposition due to the ion beam. At a fluence of 1.6×10^{13} ions cm^{-2} (Figure 2(c)), particulate nano-sized structures are seen on the NFs. These are graphene nanoparticles that began to coalesce. During irradiation, there is release of hydrogen gas, which may create defects in the polymer and lead to ag-

glomeration of nanoparticles of the filler material. Ali et al. [23], for instance, observed the formation of metal particles clusters and craters due to the release of hydrogen gas during irradiation of polyaniline-Au composites.

Closer examination of the SEM images reveals a solid layer beneath the nanofiber network that gradually grows to the surface. At fluences beyond 1.6×10^{13} ions cm^{-2}, this layer becomes fully exposed and exhibits a granular surface, as shown in Figure 2(d)-(e). The density of this layer suggests that its formation was due to a combination of polymer chain cross-linking (or gelling) and the compaction effect of the SHI beam. The gaseous release might have left behind cross-linked carbon-based free radicals in a dense network near the thin film interface. Additionally, localized heating from the SHI beam could have caused recrystallization and related processes [36], leading to the loss of the well-defined fibrous structure of PANI.

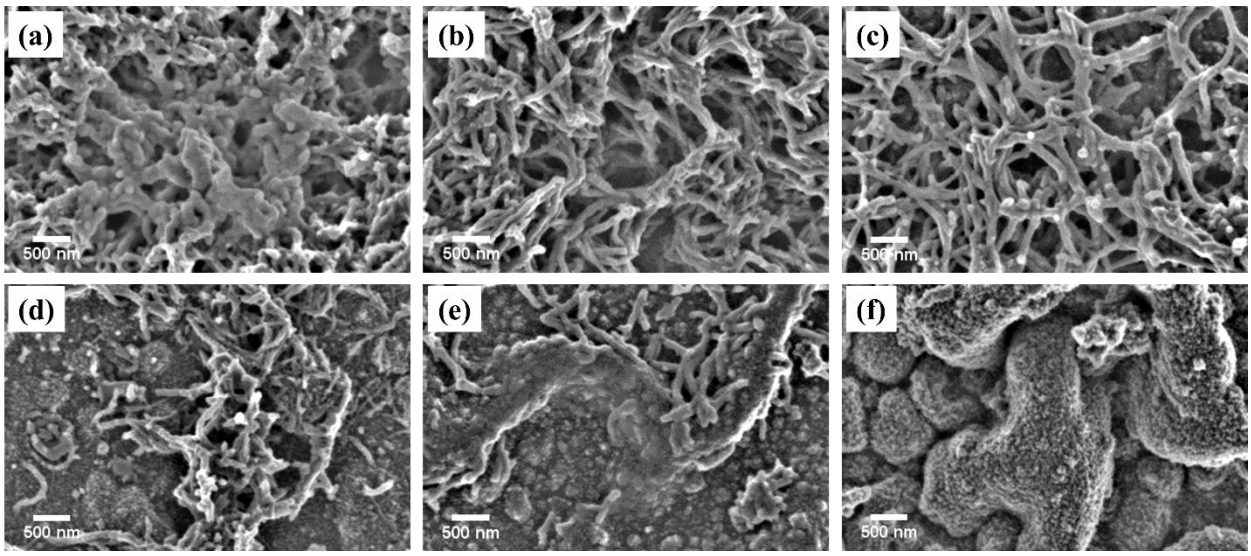

Figure 2: SEM images of PANI-G NC film samples irradiated at different fluences: (a) 5.4, (b) 11, (c) 16, (d) 21, (e) 43, and (f) 64 × 10^{12} ions/cm2. Each image shows the morphology of the sample after irradiation at the specified fluence.

3.2. Raman Spectroscopy

Raman spectroscopy is a rapid, nondestructive, and highly sensitive tool for probing defects in nanostructured sp^2 carbon systems. In this study, Raman spectroscopy was utilized to investigate the effect of graphene incorporation in PANI films as well as to understand the changes in the molecular structure of these films when subjected to different doses of 36 MeV Cu^{8+} ions. To obtain more uniform statistics from both the reduced and oxidized forms of PANI, a 532 nm excitation laser was used, as recommended by Mažeikienė and others [37]. Figure 3 displays Raman spectra of GF and unirradiated films of PANI and PANI-G, along with those of PANI-G NCs irradiated at different fluences ranging from 5.4 to 64 × 10^{12} ions/cm^2.

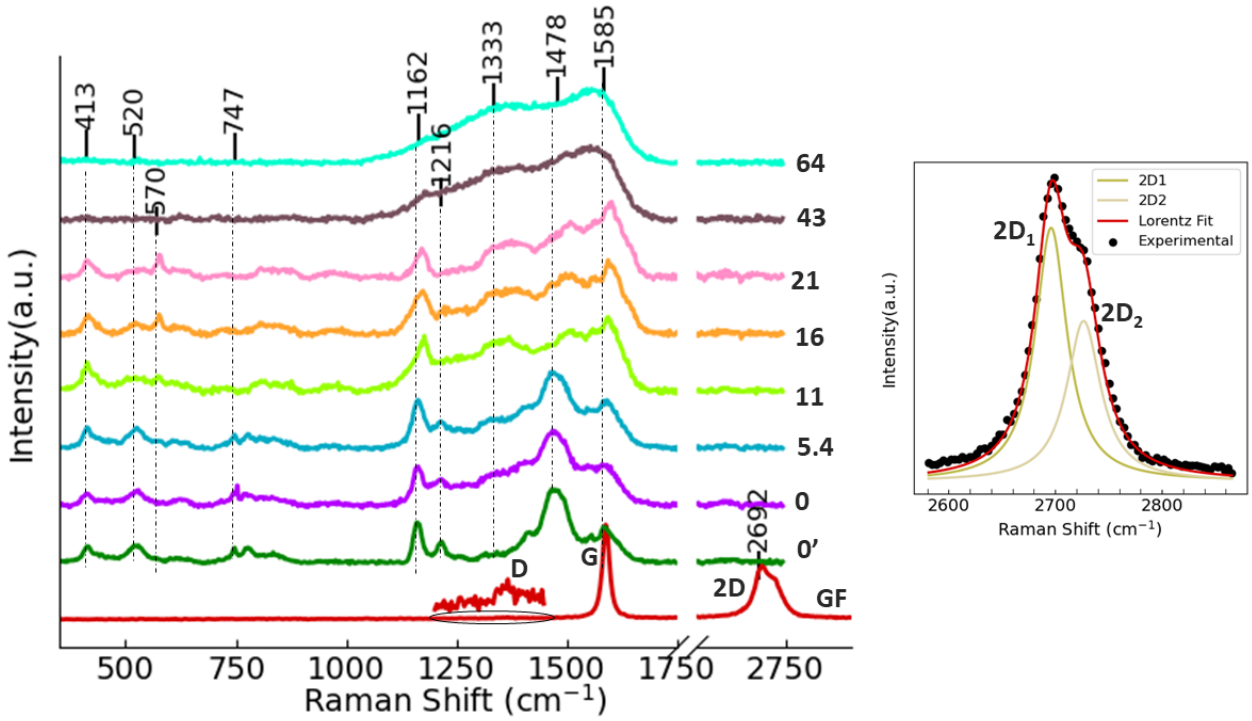

Figure 3: Raman spectra of graphene foam (GF), unirradiated PANI (0'), unirradiated PANI-G (0), and PANI-G NC films irradiated at different fluences. The fluences are represented by the

label on each plot in units of ×10^{12} ions/cm^2. The insert is a deconvoluted Lorentzian fit for the 2D band of GF. (A color version of this figure can be viewed online.)

The GF spectrum shows expected features [25,38,39] such as the G peak at 1587 cm^{-1} and the 2D band at 2692 cm^{-1}. A very weak D mode is also present around 1360 cm^{-1} showing that the graphene synthesized was of good quality. In graphitic systems, the D band in Raman spectra indicates defects and disorder in the graphene lattice, while the G band is associated with in-plane vibrations of sp^2 hybridized carbon atoms. The 2D band, on the other hand, represents second order vibrations at the Brillouin zone boundary [40]. The number of graphene layers can be estimated from the analysis of the G and 2D bands. One sensitive indicator is the ratio of their peak intensities, I_G/I_{2D}, and the symmetry and position of the 2D band. The symmetry can be determined by deconvoluting the 2D band into two Lorentzian peaks, $2D_1$ and $2D_2$, as shown in the insert of Figure 3. The positions, FWHM values, and intensity ratios of these peaks provide information about the number of graphene layers. In this study, the I_G/I_{2D} ratio was found to be 1.72; the peak position/FWHM of $2D_1$ was 2696 cm^{-1}/36.14; the peak position/FWHM of $2D_2$ was 2727 cm^{-1}/38.74; and the intensity ratio I_{2D2}/I_{2D1} was 0.632. According to Singh et al. [41], these values indicate that the number of layers in the synthesized graphene was between 7 and 12 (multi-layer graphene). Furthermore, the average size of sp^2 domains was computed, following the approach in [42], and found to be 32.7 nm.

The spectrum of unirradiated pure PANI (PANI 0) exhibits characteristic peaks, and their assignments are summarized in Table 1, following published literature [43–48]. To a large extent, these bands maintain their positions in the unirradiated PANI-G NC spectrum (PANI-G 0), with the intensity of some peaks slightly increased, indicating that interactions between PANI and graphene enhance the Raman scattering cross-section of certain signals. Notably, the G mode of graphene

at 1589 cm^{-1} overlaps with the stretching vibrations of quinonoid rings in pure PANI at 1585 cm^{-1}, causing a broadening of this band in the spectrum of the composite, PANI-G 0. This observation further confirms the existence of PANI-graphene interactions. The strongest evidence of successful composite synthesis is perhaps the significant increase in the intensity of the bands in the frequency range 1300 – 1370 cm^{-1}. This region covers the stretching vibrations of C~N $^{+\bullet}$ groups (where '~' denotes a bond intermediate between the single and double bonds) in PANI around 1333 cm^{-1} and the defect-induced D mode of graphene at 1360 cm^{-1}. These features indicate the presence of polarons in PANI and defects in graphene, respectively. The incorporation of graphene in PANI would therefore cause both of these effects, as reported by Mohamed's group [34]. They attributed this to the coupling between PANI and graphene via π–π and electrostatic interactions, which change the hybridization of carbon atoms from sp^2 to sp^3. This also explains why the 2D band of graphene is not visible in the PANI-G NC spectrum, as it is suppressed by the presence of PANI [34,49].

Table 1: Positions and Assignment of Raman Bands in the Spectra of graphene and PANI/PANI-G films [a]

Raman Shift (cm^{-1})		**Band Assignment**	
Graphene	**PANI/PANI-G**	**Graphene**	**PANI**
	413		C– H wag (o.p.) [44]
	520		(C~C) ring def (o.p) [45]
	747		Q def. (o.p), Phz [44]
	777		ring def in EB [46]

	837		(C∼C) def in Q (o.p), C– H wag (o.p.) [44,46]
	1162		$\delta(C-H)_Q$ [43,45]
	1174		$\delta(C-H)_{SQ}$ [45–47]
	1216		$\nu(C-N)_Q$ [45,47]
	1252		$\nu(C-N)_B$ [43,45,47]
	~1333		$\nu(C{\sim}N^{+\cdot})$ in p [43,45,46,48]
1360		D [25,38,39]	
	~1404		phz, $\nu(C-N)$ p − p [43–45]
	1470		$\nu(C=N)_Q$ [43,45,46]
	1561		$\nu(C-C)_Q$[43,45,46]
1589	1585	G [25,38,39]	$\nu(C=C)_Q$ [43,45,47]
	1609		$\nu(C{\sim}C)_B$[43,45,46]
2692		2D [25,38,39]	

[a] Abbreviations: wag, wagging bending vibration; o.p, out of plane; def, deformations; ν, stretching; δ, in-plane bending; B, benzenoid ring; Q, quinonoid ring; SQ, semi-quinonoid ring; p, polarons; p-p, polaron pair; phz, phenazine-like ring; ~, bond inter-mediate between the single and double bonds.

Upon treatment with different fluences of 36 MeV Cu^{8+} ions, a discernable trend is observed in the evolution of the Raman spectra of PANI-G NC films, demonstrating a systematic change in conformational structure as a function of irradiation fluence. Irradiated pure PANI shows a similar

trend, albeit at a slower rate during the initial stages, as depicted in Figure S2, under Supplementary Information. This provides further support and confirms the catalytic role played by graphene.

Analysis of the PANI-G NC spectra in Figure 3 as irradiation fluence increases reveals the following features and trends:

The peak at 1470 cm^{-1}, representing C-N stretching vibrations of non-protonated di-imine units in emeraldine PANI [49], decreases in intensity. Simultaneously, the band at 1585 cm^{-1}, which corresponds to a combination of C=C stretching modes in the quinonoid ring of PANI and the G mode of vibration in graphene (GF), gains prominence. At a fluence of 11×10^{12} ions/cm^2, the 1470 cm^{-1} band shifts slightly to ~1500 cm^{-1}, while the band previously at 1585 cm^{-1} moves to ~1600 cm^{-1}, with a subtle shoulder appearing at 1610 cm^{-1} (see PANI-G 16). The shift of the 1470 cm^{-1} band to ~1500 cm^{-1} can be attributed to the oxidation of emeraldine PANI to the more conductive form, emeraldine salt. This is in line with earlier studies [45,50] which have linked resonance modes around 1500 cm^{-1} to stretching oscillations of semi-quinone protonated di-imine units. Additionally, the shift of the band previously at 1585 cm^{-1} to ~1600 cm^{-1} and the appearance of a shoulder at 1610 cm^{-1} are a result of the presence of another defect band, the D' band, induced by ion bombardment. This observation is substantiated by prior research [26,40,51,52], which demonstrated that SHI irradiation can broaden the G band of graphene by introducing a D' peak through intravalley double resonance processes in the presence of defects.

The broad band centered at 1333 cm^{-1}, initially enhanced by graphene doping, becomes even more pronounced upon irradiation. This region is characteristic of C~N+• vibrations in the polaronic lattice [45,49], responsible for the electrical conductivity of emeraldine salt PANI. With increasing irradiation exposure, the peak gradually shifts towards the position of the D mode of GF (1365 cm^{-1}), indicating the accumulation of defects in graphene, as anticipated [40,51]. Likewise, the shift

of the C-H deformations band of quinonoid rings from 1162 cm^{-1} to 1174 cm^{-1}, imputed to C-H deformation modes of semi-quinonoid rings, along with the disappearance of the peak at 1216 cm^{-1} upon increased irradiation dose, provides further evidence of PANI protonation by the ion beam.

In the low wavenumber region, certain peaks (e.g., at 520 cm^{-1} and 570 cm^{-1}) show a noticeable increase in intensity up to a fluence of 21×10^{12} ions/cm^2. In this spectral range, Raman is known to be sensitive to the crystallinity and conformational structure of the PANI backbone [10,53]. The heightened intensity of active modes in this range indicates an increase in the crystallinity of PANI-G NC, which is supported by XRD results. Spectra obtained at fluences higher than 21×10^{12} ions/cm^2 exhibit a broad envelope centered at the D and G positions of graphene, resembling the characteristics of nanocrystalline graphite [54,55]. Overall, the Raman results align with SEM observations, demonstrating that optimal morpho-structural properties are achieved at fluences between 5.0×10^{12} ions/cm^2 and 21×10^{12} ions/cm^2 due to enhanced physicochemical interactions between PANI and graphene.

3.3. XRD Results

The effect of 36 MeV Cu8+ ions on the crystal structure of PANI-G NCs was investigated using X-ray diffraction (XRD). Figure 4(a) presents the diffraction patterns of various samples, including GF, unirradiated pure PANI, unirradiated PANI-G, and PANI-G NCs exposed to different ion doses. The spectra were obtained after normalization and subtraction of the ITO/glass background. Figure 4(b) provides a magnified view of the shaded regions in Figure 4(a) for better visibility.

In the diffractogram of GF, a strong diffraction peak is observed at $2\theta = 26.9^{o}$, which corresponds to (002) crystalline graphene planes [56,57] with an interlayer spacing (d-spacing) of 33 Å. Additionally, weak peaks are observed at $2\theta = 45.1^{o}$ and 55.2^{o}, relating to (100) and (004) crystallographic planes, respectively. The presence of the (004) diffraction peak in the graphene

signature is indicative of good crystallinity and a high number of stacked layers [58]. Huh [59] proposed a model to relate the number of layers, $N_{L,}$ in multi-layer graphene to its corresponding thickness, D_{GP}, as,

$$N_L = \frac{D_{GP} + d_{002}}{d_{002}} \quad (1)$$

with d_{002} representing the d-spacing of (002) planes. The thickness, D_{GP}, is essentially the crystalline domain length, or the crystallite size, calculated from the Scherrer formula [60],

$$D_{GP} = \frac{K\lambda}{\beta_{002} cos(\theta)} \quad (2)$$

where β_{002} is the FWHM of the (002) peak (in radians), λ = 1.54184 Å the wavelength of the CuK_{α} X-ray, θ is the scattering angle, and K is a constant dependent on the crystallite shape. Huh determined the value of K for this analysis to be 0.28 [59]. Using this value, the number of layers in GF was computed and found to be ~10, in agreement with our Raman results (cf. Section 3.2).

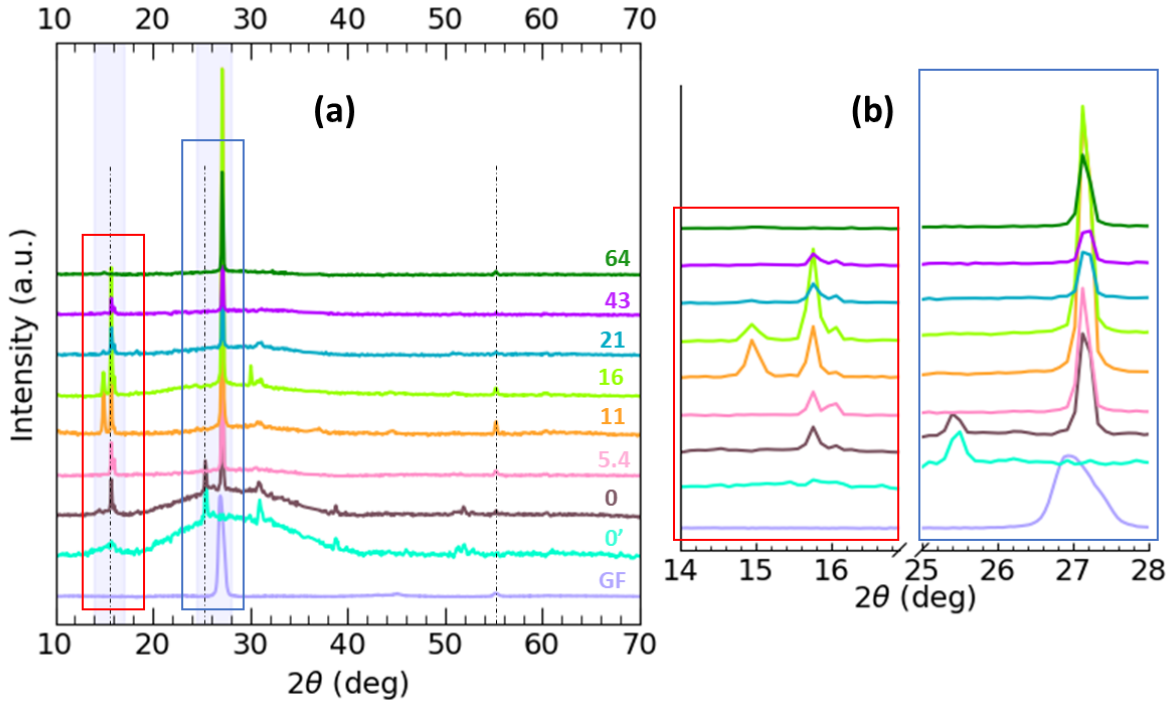

Figure 4: (a) XRD patterns for graphene foam (GF), pure unirradiated PANI (0'), and PANI-G NC films exposed to different ion doses (0, 5.4, 11, 16, 21, 43, and 64 × 10^{12} ions/cm2) (b) Up-close view of the shaded portions of Figure 4(a). (A color version of this figure can be viewed online.)

Polymers typically exhibit a semi-crystalline nature, with crystalline regions (or crystallites) intersperse in an amorphous medium [61]. This characteristic is reflected in their XRD patterns, where sharp peaks superimposed on broad backgrounds are observed. The sharp and narrow peaks indicate the presence of crystalline domains, whereas the broad and diffuse peaks signify the presence of amorphous phases. In the XRD profile of pure PANI (0' in Figure 4(a)), sharp peaks can be observed at 2θ positions of 15.8, 25.5, 31.0, 38.8, 46.0, and 52.0 º, overlaid on a broad halo centered around 27º. Acid-doped PANI has been proposed to have a pseudo-orthorhombic unit cell structure [62,63]. The peaks at 2θ ~15 º are assigned to (100) diffractions with d-spacings

ranging from 5.6 to 5.9 Å. Meanwhile, interplanar distances around 3.5 Å (2θ ~25) are linked to diffractions from the (110) planes, indicating crystallinity due to parallel and perpendicular periodicity among adjacent phenyl rings [64]. Reflections in the vicinity of 27 º (d-spacing values ~3.3 Å) for (111) planes are attributed to diagonal face-to-face inter-chain stackings. According to Varma et al. [65], these stackings promote a planar chain conformation that improves π –π interactions and facilitates charge transport associated with the dopant ions between the polymer chains.

The 2θ scan of the unirradiated PANI-G composite film (0) shows notable changes compared to pure PANI. The amorphous halo attenuates, the peak around 15.8 º sharpens, and two new reflections emerge: a prominent peak at 2θ = 27.1 º and a less pronounced one at 2θ = 14.9 º. These changes suggest enhanced crystallinity stemming from the insertion of dopant graphene nanofillers between PANI chains. The peak at 2θ = 27.1 º, slightly above that of GF (26.9 º), and coinciding with the centroid of the halo in pure PANI, demonstrates a composite behavior owing to interactions between PANI and graphene. These interactions may have led to an ordering of the (111) crystallographic planes of PANI. Similarly, the emergence of the 14.9 º peak entails the formation of new oriented domains in the [002] direction [66]. The slight shift of the 27.1 º signal to a higher 2θ position relative to GF implies that graphene was likely deposited on the PANI surface rather than PANI being intercalated between graphene sheets, as intercalation would have increased interlayer separation (d-spacing).

Upon irradiation with swift Cu^{8+} ions, no shifts are detected in the positions of diffraction maxima signaling minimal alterations in the lattice parameters. However, there is an increase in the intensity of peaks up to a fluence of 16×10^{12} ions/cm^2. The observed increase in diffraction intensity depicts an augmentation in the crystallinity of the composite films and can be ascribed to

the rearrangement of molecular bonds resulting from rapid and localized excitation/ionization events during SHI irradiation. These events may produce well-aligned regions through chain folding, cross-linking or helix formation [9,12,67], and could also enhance interactions between PANI and graphene. At high fluences (beyond 16×10^{12} ions/cm^2), peak intensities reduce, signifying amorphization due to polymer degradation from excessive electronic energy deposition. Notice that at the highest fluence, there is almost a complete loss of the PANI character, but the graphitic signature is intensified. This trend of increased and then diminished crystallinity upon ion irradiation of polymeric materials has been reported by other research groups [9,11,20,67]. The irradiation response of pure PANI follows this pattern and is included in the supporting information as Figure S3.

In XRD analysis, parameters that give quantitative insights into structural characteristics include the percentage crystallinity and the crystallite size [60]. The percentage crystallinity, ϕ_c, reflects the degree of crystallinity and is defined as,

$$\phi_c = \left(\frac{\sum I_c}{\sum I_{tot} - \sum I_{bgr}} \right) \times 100 \tag{3}$$

where $\sum I_{tot}$ is the integrated area of the whole X-ray diffractogram, and $\sum I_c$ and $\sum I_{bgr}$ are the integral areas of the crystalline signals and Compton background, respectively. The crystallite size, on the other hand, denotes the physical extent of crystalline domains and is evaluated from the Scherrer formular (Equation (2)). In cases where peaks are not well-resolved or symmetrical, it is advised to use the Integral Breadth [68], L_{hkl}, in place of the FWHM, i.e.,

$$D_{hkl} = \frac{K\,\lambda}{L_{hkl}\,cos(\theta)} \tag{4}$$

L_{hkl} is defined as the ratio of peak area to peak height. In Table 2, values of percentage crystallinity and crystallite size as determined from the above analysis for different samples are listed. For the analysis of crystallite size, we used the two most intense peaks ($2\theta_1$ and $2\theta_2$) in each sample's diffraction pattern and computed their average. The obtained values of crystallinity are comparable to those reported by Ramola et al. [67] when they irradiated PANI with 50 MeV Li^{3+} ions, but the crystallite sizes observed in the present work are larger. At its highest, the crystallinity of PANI-G NC increased by 77%, while the crystallite size showed a substantial growth of up to 481% compared to pure PANI. It is curious to note that the highest crystallite size coincides with the sp^2 domain length found by Raman (cf. Section 3.2). Higher crystallinity levels are strongly linked with improved electrical conductivity [12].

Table 2: Crystallite size and percentage crystallinity in unirradiated PANI (0') and PANI-G NC films impinged with different fluences of 36 MeV Cu^{8+} ions. The NC samples are labeled according to their irradiation doses in units of $\times 10^{12}$ ions/cm^2. For crystallite size analysis, the two most intense peaks ($2\theta_1$ and $2\theta_2$) in the diffraction pattern of each sample were used from which the average was computed.

Sample	Crystallite size							Crystallinity (%)
	Diffraction peak 2θ (°)		Integral Breadth L		Crystallite sizes D (nm)		Average crystallite size (nm)	
	$2\theta_1$	$2\theta_2$	L_1	L_2	D_1	D_2	D_{av}	
0'	15.8	25.5	2.05	1.10	4.1	7.8	5.9	30
0	15.8	27.1	0.44	0.46	19.0	18.4	18.7	40

5.4	15.8	27.1	0.41	0.29	20.5	29.5	25.0	48
11	15.8	27.1	0.22	0.34	39.6	24.5	32.0	51
16	15.8	27.1	0.22	0.28	38.5	30.0	34.3	53
21	15.8	27.1	0.40	0.43	20.8	19.2	20.0	35
43	15.8	27.2	0.46	0.40	17.9	20.7	19.3	28
64	14.9	27.1	0.95	0.31	8.8	26.7	17.8	31

3.4. UV-Vis

To examine the impact of Cu8+ projectiles on the optical properties of PANI-G NC films, UV-Vis spectroscopy was employed. This technique measures the absorption or transmission of light by a sample over a range of wavelengths and can provide valuable information about the electronic structure, energy bandgap, and carbon cluster characteristics in irradiated polymers [69]. Figure 5(a) compares the absorption spectra of virgin (unirradiated) PANI and PANI-G. It is important to note that GF was opaque, which limited its optical analysis. As shown in Figure 5(a), both spectra have three distinct peaks, characteristic of PANI in its emeraldine salt form [70]. The first peak, at 330 nm in the UV region, corresponds to the π-π* electronic transition between the HOMO and LUMO of the benzenoid rings of PANI. The second peak, at 438 nm in the visible region, and the broad band extending into the near-infrared region (~850 nm), represent excitations of π electrons to the polaron band. Stafstrom and team [71] noted that unlike other conducting polymers, which have two defect bands within the band gap due to destabilization of the HOMO and stabilization of the LUMO, PANI forms a polaron lattice when unstable bipolarons separate into two polarons on a polyemeraldine chain. Thus, the bands at 438 nm and ~850 nm are assigned to π-polaron and polaron-π* transitions, respectively. It can also be observed from Figure 5(a) that the PANI-G

composite exhibits higher optical absorption than pure PANI and that the edge of the 438 nm band in the PANI-G composite is significantly redshifted in comparison to PANI. From the literature [72], the UV-Vis absorption of graphene nanostructures (usually in solution) is due to surface plasmon resonance (SPR) of free electrons and has a maximum between 230 and 300 nm. The observed redshift in the PANI-G composite is therefore not solely due to graphene but rather indicates a strong interaction between graphene and PANI, confirming successful composite formation.

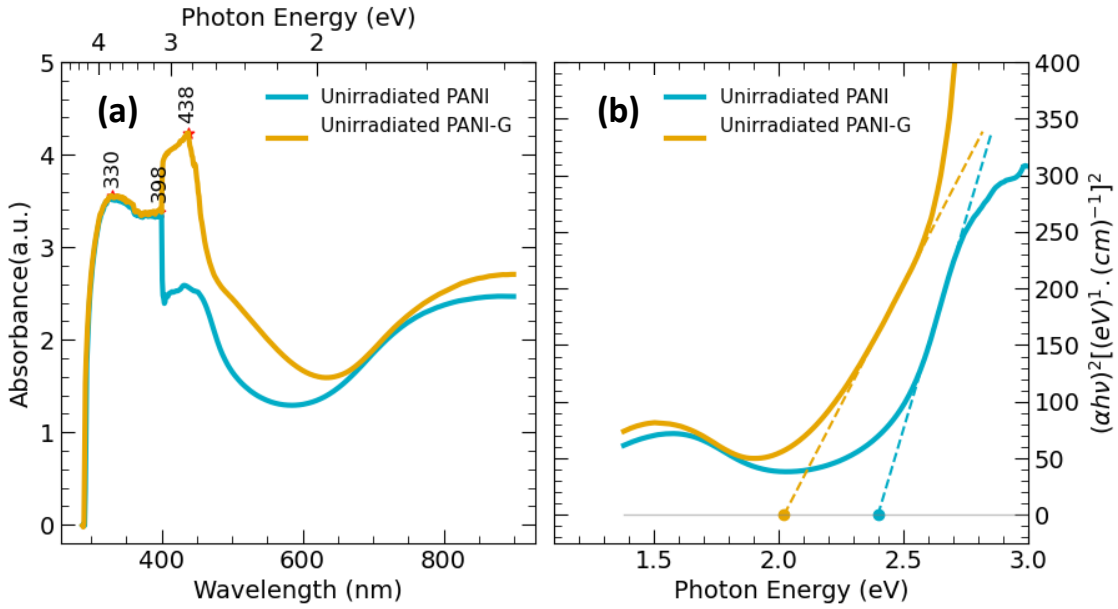

Figure 5: UV-Vis absorbance spectra and corresponding Tauc plots of unirradiated PANI and PANI-G NC films (a, b). The composite shows increased optical absorption (cf. (a)) and reduced bandgap energy (cf. (b)). *(A color version of this figure can be viewed online.)*

Optical band edge can be correlated with energy bandgap, E_g , through the Tauc method [73]. PANI is known to have a direct bandgap [13], whereby the optical absorption coefficient (α) is related to the photon energy (hν) by the equation,

$$\alpha h\nu = A(h\nu - E_g)^{1/2} \quad (5)$$

where A is a constant and E_g is the energy bandgap. Hence, plotting $(\alpha h\nu)^2$ against $h\nu$ and extrapolating the linear region to the abscissa, as shown in Figure 5(b), gives E_g. From the Tauc plots in Figure 5(b), it is evident that there is a considerable reduction in the bandgap of PANI after incorporation of graphene, from 2.40 eV to 2.02 eV. This decrease aligns with the findings of Abutalib [74] when they loaded nanoparticles of graphene oxide in PANI/PMMA blends. The reduced bandgap was referred to an introduction of defect states in the forbidden energy gap resulting from the formation of charge transfer complexes.

To unveil the effects of ion beam irradiation on the optical properties of PANI-G NC films, Figure 6 illustrates the fluence-dependent variations in the visible to NIR region. The UV region did not show any changes and is therefore not shown. Panel 6(a) presents the spectral absorbance and panel 6(b) displays the Tauc plots. With increasing fluence, there is a general increase in absorbance in the optical region and the absorption edge leading up to the 450 nm peak gradually 'flattens'. According to Ramola et al. [11], a rise in absorption intensity in this spectral region reflects an increase in the number of charge carriers, such as free radicals and ions, in the polymer film, which in turn suggests improved conductivity. As shown in Figure 6(b), the bandgap decreases with ion dose; starting at 2.02 eV for the unirradiated composite film, to 2.01, 1.67, 1.52, 1.47, 1.46, and finally to 1.40 eV at the highest integrated flux. Reduction in the optical bandgap of PANI following ion irradiation has been observed [17]. It is credited to chain scission (degradation) and cross-linking at low to moderate doses, as well as to carbonization at higher fluencies [75].

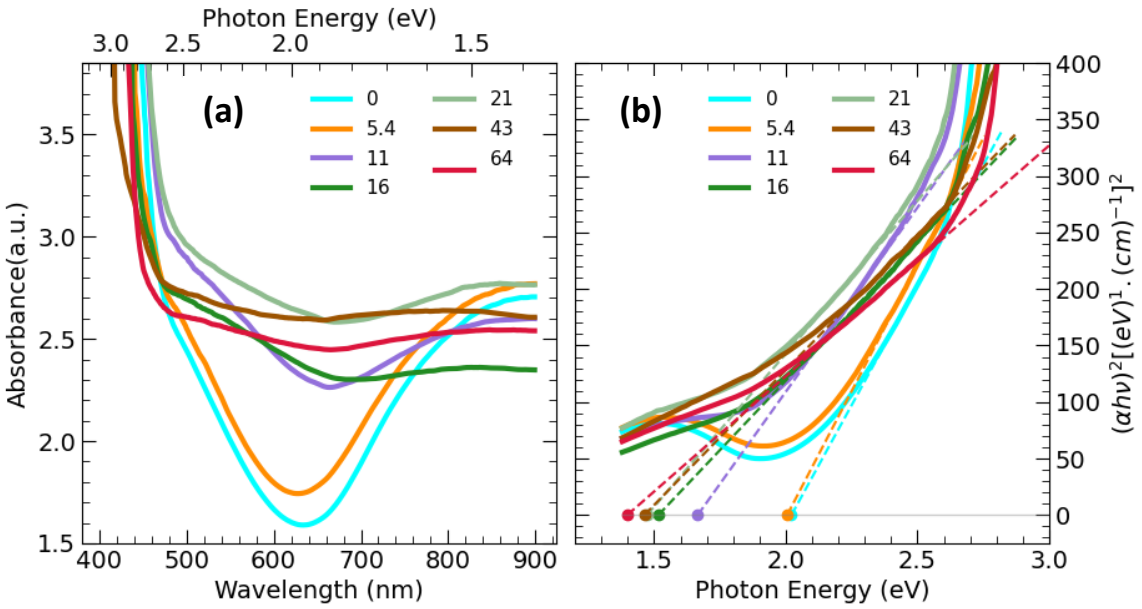

Figure 6: Optical absorption spectra (a) and corresponding Tauc plots (b) of PANI-G NCs irradiated at different fluences. The Tauc plots were used to determine the optical bandgap of the materials. The films exhibit good engineerability in bandgap as a result of ion-beam irradiation. (A color version of this figure can be viewed online.)

When energetic ions pass through a polymer, they transfer electronic energy to the material, creating highly excited carbon atoms along their tracks, which condense into compact nanometric clusters [69]. These carbonaceous clusters can endow materials with high electrical conductivity and good optical transparency. It has been shown [76] that for polymers containing aromatic rings, the number of rings, *M*, in such clusters is related to the optical bandgap by,

$$E_g = \frac{5.8}{\sqrt{M}}\ eV \qquad (6)\ (a)$$

Fink et al. [69] argued that after irradiation, a significant number of bonds are destroyed along the ion track, and application of Equation (6)(a) leads to an underestimation of the number, *N*, of

carbon atoms per cluster. Thus, by assuming the structure of a buckminsterfullerene, C_{60}, cluster instead of C_6 rings, they obtained the relation,

$$E_g = \frac{34.3}{\sqrt{N}}\ eV \qquad (6)\ (b)$$

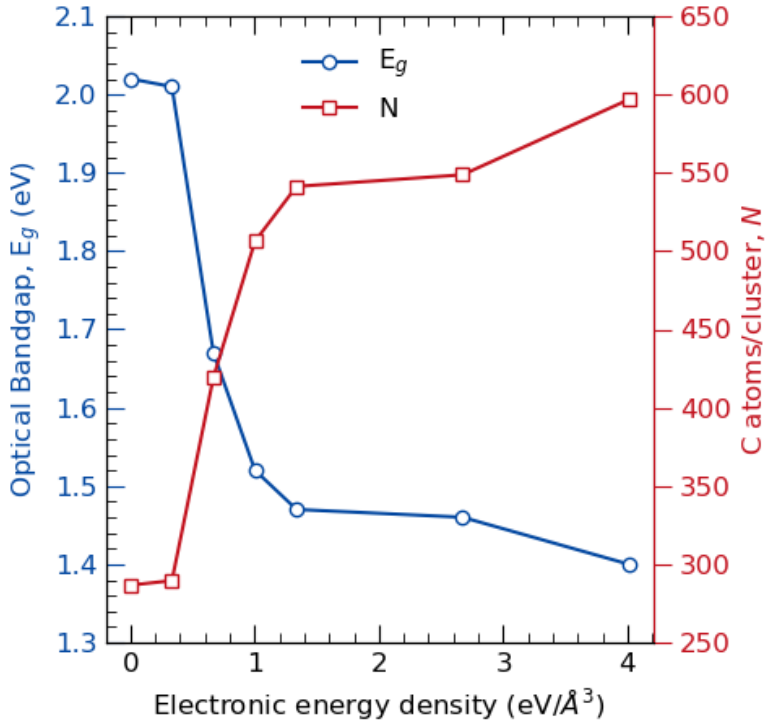

Figure 7: Variation of energy bandgap and cluster size (number of carbon atoms per cluster) with mean electronic energy transferred to PANI-G NCs. (A color version of this figure can be viewed online.)

In Figure 7, energy bandgaps evaluated at different fluences and their corresponding cluster sizes are correlated with the mean deposited energy density (product of linearly transferred electronic energy and fluence) via Equation 6(b). The figure shows that remarkable ion-beam induced cluster formation commences at a mean deposited energy density of ~ 0.33 eV/Å^3. This result supports the study by Firk et al. [69], which indicates that strong cluster formation in polymers is triggered

only above a threshold electronic energy density of around 10^{-2} to 10^{-1} eV/Å^3. Hence, the carbon enriched domains are mainly responsible for the observed decrease in energy bandgap.

4. Conclusion

The effects of SHI irradiation on the structural and optical properties of PANI-G NC films have been thoroughly investigated. Our results indicate that interactions between PANI and graphene cause initial changes which are further enhanced by ion exposure. From SEM, irradiation with 36 MeV Cu^{8+} led to the formation of a porous interconnected network at lower fluences, with graphene granules attached to PANI NFs, and a dense and compact granular structure at higher fluences. Raman spectroscopy revealed changes indicating a polaronic lattice structure in emeraldine salt PANI and an accumulation of defects in graphene. These changes were caused by molecular bond rearrangement from SHIs through chain folding, cross-linking, or helix formation. At fluences exceeding 2.1×10^{13} ions/cm^2, the spectra displayed a broad envelope centered at the D and G positions of graphene, the hallmark of nano-crystalline graphite. XRD showed that with increasing fluence, the crystallinity and the crystallite size of the PANI-G NC film increased by up to 77% and 481%, respectively, at the total flux of 1.6×10^{13} ions/cm^2. Beyond this, a decrease in these values was recorded. Irradiation with high-energy ions significantly increased the optical absorption of PANI-G NC films and reduced the bandgap from 2.02 eV, in the unirradiated film, to 1.40 eV at the highest dose. This decrease in bandgap is attributed to the formation of carbonaceous clusters along the latent tracks of ions due to electronic energy transfer. The threshold for cluster formation was found to be approximately 0.33 eV/Å^3. Overall, this study demonstrates that the characteristics of PANI-G NC films vary continuously with change in ion fluence, suggesting that SHI irradiation can be used to precisely control the structural and optical properties of these films to tailor them for specific applications.

CRediT Authorship Contribution Statement

D.C. Chilukusha: Conceptualization, Methodology, Investigation, Data curation, Formal analysis, Writing - original draft. **J.J. Mboukam**: Data curation, Formal analysis, Writing -review & editing. **V.M. Maphiri**: Data curation, Formal analysis, Writing -review & editing. **N. Manyala**: Methodology, Resources, Writing -review & editing, Supervision, Project administration, Funding acquisition. **M. Msimanga**: Conceptualization, Methodology, Resources, Writing -review & editing, Supervision, Project administration, Funding acquisition.

Declaration of Competing Interest

The authors declare that there are no known competing financial interests or personal relationships that could have influenced the work reported in this paper.

Acknowledgements

The authors would like to acknowledge the Tshwane University of Technology (through the PV NanoComposites R&D Platform), NRF-iThemba LABS and the University of Pretoria for financial and infrastructural support. The lead author wishes to thank his home institution, Mulungushi University, for financial support.

Declaration of generative AI and AI-assisted technologies in the writing process

During the preparation of this work, the author(s) used Microsoft Bing to improve the readability of the content. After using this tool, the author(s) reviewed and edited the content as needed and take full responsibility for the content of the publication.

Data availability

The raw data required to reproduce these findings are available to download from [https://data.mendeley.com/datasets/62x535z38b/draft?a=6607cf45-005f-4d75-8cfa-10484d915443].

References

[1] K. Namsheer, C.S. Rout, Conducting polymers: A comprehensive review on recent advances in synthesis, properties and applications, RSC Advances. 11 (2021) 5659–5697.

[2] A.G. Olabi, M.A. Abdelkareem, T. Wilberforce, E.T. Sayed, Application of graphene in energy storage device – A review, Renewable and Sustainable Energy Reviews. 135 (2021) 110026. https://doi.org/10.1016/j.rser.2020.110026.

[3] S.K. Tiwari, S. Sahoo, N. Wang, A. Huczko, Graphene research and their outputs: Status and prospect, Journal of Science: Advanced Materials Devices. 5 (2020) 10–29.

[4] H. Huang, H. Shi, P. Das, J. Qin, Y. Li, X. Wang, F. Su, P. Wen, S. Li, P. Lu, F. Liu, Y. Li, Y. Zhang, Y. Wang, Z. Wu, H. Cheng, The Chemistry and Promising Applications of Graphene and Porous Graphene Materials, Adv. Funct. Mater. 30 (2020) 1909035. https://doi.org/10.1002/adfm.201909035.

[5] M. Beygisangchin, S. Abdul Rashid, S. Shafie, A.R. Sadrolhosseini, H.N. Lim, Preparations, Properties, and Applications of Polyaniline and Polyaniline Thin Films—A Review, Polymers. 13 (2021) 2003. https://doi.org/10.3390/polym13122003.

[6] E. Eskandari, M. Kosari, M.H. Davood Abadi Farahani, N.D. Khiavi, M. Saeedikhani, R. Katal, M. Zarinejad, A review on polyaniline-based materials applications in heavy metals removal and catalytic processes, Separation and Purification Technology. 231 (2020) 115901. https://doi.org/10.1016/j.seppur.2019.115901.

[7] A.T. Lawal, Recent progress in graphene based polymer nanocomposites, Cogent Chemistry. 6 (2020) 1833476.

[8] A.D. Scaccabarozzi, A. Basu, F. Aniés, J. Liu, O. Zapata-Arteaga, R. Warren, Y. Firdaus, M.I. Nugraha, Y. Lin, M. Campoy-Quiles, N. Koch, C. Müller, L. Tsetseris, M. Heeney, T.D. Anthopoulos, Doping Approaches for Organic Semiconductors, Chem. Rev. 122 (2022) 4420–4492. https://doi.org/10.1021/acs.chemrev.1c00581.

[9] J. Hazarika, A. Kumar, Swift Heavy Ion Irradiation Effects on the Properties of Conducting Polymer Nanostructures, in: V. Kumar, B. Chaudhary, V. Sharma, K. Verma (Eds.), Radiation Effects in Polymeric Materials, Springer International Publishing, Cham, 2019: pp. 193–242. https://doi.org/10.1007/978-3-030-05770-1_6.

[10] A. Kumar, S. Banerjee, Swift heavy ion irradiation: A novel technique for tailoring the size of polyaniline nanofibers, International Journal of Nanoscience. 10 (2011) 161–165.

[11] R.C. Ramola, S. Chandra, Ion Beam Induced Modifications in Conducting Polymers, DDF. 341 (2013) 69–105. https://doi.org/10.4028/www.scientific.net/DDF.341.69.

[12] S. Chandra, S. Annapoorni, R.G. Sonkawade, P.K. Kulriya, F. Singh, D.K. Avasthi, J.M.S. Rana, R.C. Ramola, Interaction of oxygen (O+7) ion beam on polyaniline thin films, Indian J Phys. 83 (2009) 943–947. https://doi.org/10.1007/s12648-009-0052-9.

[13] S. Banerjee, A. Kumar, Swift heavy ion irradiation induced modifications in the optical band gap and Urbach's tail in polyaniline nanofibers, Nuclear Instruments and Methods in Physics Research Section B: Beam Interactions with Materials and Atoms. 269 (2011) 2798–2806. https://doi.org/10.1016/j.nimb.2011.09.004.

[14] S. Banerjee, A. Kumar, Micro-Raman studies of swift heavy ion irradiation induced structural and conformational changes in polyaniline nanofibers, Nuclear Instruments and Methods in Physics Research Section B: Beam Interactions with Materials and Atoms. 268 (2010) 2683–2687. https://doi.org/10.1016/j.nimb.2010.06.003.

[15] A. Kumar, S. Banerjee, J.P. Saikia, B.K. Konwar, Swift heavy ion irradiation induced enhancement in the antioxidant activity and biocompatibility of polyaniline nanofibers, Nanotechnology. 21 (2010) 175102. https://doi.org/10.1088/0957-4484/21/17/175102.

[16] A. Srivastava, V. Singh, A. Chandra, K. Witte, U.W. Scherer, T.V. Singh, Electrical conductivity studies of swift heavy ion modified PVC and PVC–PANI composite, Nuclear Instruments and Methods in Physics Research Section B: Beam Interactions with Materials and Atoms. 245 (2006) 277–280. https://doi.org/10.1016/j.nimb.2005.11.114.

[17] M.M. Abdelhamied, A. Atta, A.M. Abdelreheem, A.T.M. Farag, M.A. El Sherbiny, Oxygen ion induced variations in the structural and Linear/Nonlinear optical properties of the PVA/PANI/Ag nanocomposite film, Inorganic Chemistry Communications. 133 (2021) 108926. https://doi.org/10.1016/j.inoche.2021.108926.

[18] A. Srivastava, V. Singh, C. Dhand, M. Kaur, T. Singh, K. Witte, U. Scherer, Study of Swift Heavy Ion Modified Conducting Polymer Composites for Application as Gas Sensor, Sensors. 6 (2006) 262–269. https://doi.org/10.3390/s6040262.

[19] P. Sonar, A.L. Sharma, A. Chandra, K. Muellen, A. Srivastava, Synthesis and study of conductivity behaviour of blended conducting polymer films irradiated with swift heavy ions of silicon, Current Applied Physics. 3 (2003) 247–250. https://doi.org/10.1016/S1567-1739(02)00210-9.

[20] H.K. Patil, M.A. Deshmukh, S.D. Gaikwad, G.A. Bodkhe, K. Asokan, M. Yasuzawa, P. Koinkar, M.D. Shirsat, Influence of oxygen ions irradiation on Polyaniline/Single walled carbon nanotubes nanocomposite, Radiation Physics Chemistry. 130 (2017) 47–51.

[21] H.K. Patil, M.A. Deshmukh, G.A. Bodkhe, S.M. Shirsat, K. Asokan, M.D. Shirsat, Reinforcement of polyaniline and poly-(o-toluidine) with SWNTs and tuning of their physicochemical properties by heavy ion beams, Applied Physics A. 124 (2018) 1–11.

[22] H.K. Patil, M.A. Deshmukh, G.A. Bodkhe, S.M. Shirsat, K. Asokan, M.D. Shirsat, Dimethylglyoxime modified swift heavy oxygen ions irradiated polyaniline/single walled carbon nanotubes composite electrode for detection of cobalt ions, Mater. Res. Express. 5 (2018) 065048. https://doi.org/10.1088/2053-1591/aaccb3.

[23] Y. Ali, V. Kumar, R.G. Sonkawade, A.S. Dhaliwal, Effect of swift heavy ion beam irradiation on Au–polyaniline composite films, Vacuum. 90 (2013) 59–64. https://doi.org/10.1016/j.vacuum.2012.10.001.

[24] W. Naqash, K. Majid, Synthesis, Characterization and Study of Effect of Irradiation on Electronic Properties of Polyaniline Composite with Metal Complex of Co (III), Mat. Res. 18 (2015) 1121–1127. https://doi.org/10.1590/1516-1439.035715.

[25] H. Vázquez, E.H. Åhlgren, O. Ochedowski, A.A. Leino, R. Mirzayev, R. Kozubek, H. Lebius, M. Karlušic, M. Jakšic, A.V. Krasheninnikov, J. Kotakoski, M. Schleberger, K. Nordlund, F. Djurabekova, Creating nanoporous graphene with swift heavy ions, Carbon. 114 (2017) 511–518. https://doi.org/10.1016/j.carbon.2016.12.015.

[26] J. Zeng, J. Liu, S. Zhang, J. Duan, P. Zhai, H. Yao, P. Hu, K. Maaz, Y. Sun, Graphene electrical properties modulated by swift heavy ion irradiation, Carbon. 154 (2019) 244–253. https://doi.org/10.1016/j.carbon.2019.08.006.

[27] L. Madauß, J. Schumacher, M. Ghosh, O. Ochedowski, J. Meyer, H. Lebius, B. Ban-d'Etat, M.E. Toimil-Molares, C. Trautmann, R.G.H. Lammertink, M. Ulbricht, M. Schleberger, Fabrication of nanoporous graphene/polymer composite membranes, Nanoscale. 9 (2017) 10487–10493. https://doi.org/10.1039/C7NR02755A.

[28] M. Devi, A. Kumar, Surface modification of reduced graphene oxide-polyaniline nanotubes nanocomposites for improved supercapacitor electrodes, Polymer Composites. 41 (2020) 653–667.

[29] L. Rodríguez-Pérez, M.Á. Herranz, N. Martín, The chemistry of pristine graphene, Chem. Commun. 49 (2013) 3721. https://doi.org/10.1039/c3cc38950b.

[30] K.O. Oyedotun, N. Manyala, Graphene Foam–Based electrochemical capacitors, Current Opinion in Electrochemistry. 21 (2020) 125–131.

[31] A. Fischer, F. Kaschura, Sweepme!, (2018). https://sweep-me.net.

[32] J.F. Ziegler, J.P. Biersack, M.D. Ziegler, The Stopping and Range of Ions in Solids, SRIM Software, (2013). http://www.srim.org.

[33] F. Fenniche, Y. Khane, A. Henni, D. Aouf, D. Elhak Djafri, Synthesis and characterization of PANI nanofibers high-performance thin films via electrochemical methods, Results in Chemistry. 4 (2022) 100596. https://doi.org/10.1016/j.rechem.2022.100596.

[34] F. Mohamad, Mohd Mat Zaid, J. Abdullah, R. Zawawi, H. Lim, Y. Sulaiman, Norizah Abdul Rahman, Synthesis and Characterization of Polyaniline/Graphene Composite Nanofiber and Its Application as an Electrochemical DNA Biosensor for the Detection of Mycobacterium tuberculosis, Sensors. 17 (2017) 2789. https://doi.org/10.3390/s17122789.

[35] D.K. Bandgar, G.D. Khuspe, R.C. Pawar, C.S. Lee, V.B. Patil, Facile and novel route for preparation of nanostructured polyaniline (PANi) thin films, Appl Nanosci. 4 (2014) 27–36. https://doi.org/10.1007/s13204-012-0175-8.

[36] M. Lagarde, A. de Paz, M.F. Del Grosso, D. Fasce, R. Dommarco, S. Laino, L.A. Fasce, On the comparison of changes induced in crystallinity and surface nanomechanical properties of ultra high molecular weight polyethylene by γ and swift heavy ion irradiations, Surface and Coatings Technology. 258 (2014) 293–299. https://doi.org/10.1016/j.surfcoat.2014.09.010.

[37] R. Mažeikienė, V. Tomkutė, Z. Kuodis, G. Niaura, A. Malinauskas, Raman spectroelectrochemical study of polyaniline and sulfonated polyaniline in solutions of different pH, Vibrational Spectroscopy. 44 (2007) 201–208. https://doi.org/10.1016/j.vibspec.2006.09.005.

[38] E.H. Martins Ferreira, M.V.O. Moutinho, F. Stavale, M.M. Lucchese, R.B. Capaz, C.A. Achete, A. Jorio, Evolution of the Raman spectra from single-, few-, and many-layer graphene with increasing disorder, Phys. Rev. B. 82 (2010) 125429. https://doi.org/10.1103/PhysRevB.82.125429.

[39] A. Gupta, G. Chen, P. Joshi, S. Tadigadapa, Eklund, Raman Scattering from High-Frequency Phonons in Supported *n* -Graphene Layer Films, Nano Lett. 6 (2006) 2667–2673. https://doi.org/10.1021/nl061420a.

[40] J. Zeng, J. Liu, H.J. Yao, P.F. Zhai, S.X. Zhang, H. Guo, P.P. Hu, J.L. Duan, D. Mo, M.D. Hou, Y.M. Sun, Comparative study of irradiation effects in graphite and graphene induced by swift heavy ions and highly charged ions, Carbon. 100 (2016) 16–26. https://doi.org/10.1016/j.carbon.2015.12.101.

[41] M. Singh, H.S. Jha, P. Agarwal, Growth of large sp2 domain size single and multi-layer graphene films at low substrate temperature using hot filament chemical vapor deposition, Materials Letters. 126 (2014) 249–252. https://doi.org/10.1016/j.matlet.2014.04.066.

[42] T. Yamada, M. Ishihara, M. Hasegawa, Large area coating of graphene at low temperature using a roll-to-roll microwave plasma chemical vapor deposition, Thin Solid Films. 532 (2013) 89–93. https://doi.org/10.1016/j.tsf.2012.12.102.

[43] M. Bláha, M. Bouša, V. Valeš, O. Frank, M. Kalbáč, Two-Dimensional CVD-Graphene/Polyaniline Supercapacitors: Synthesis Strategy and Electrochemical Operation, ACS Appl. Mater. Interfaces. 13 (2021) 34686–34695. https://doi.org/10.1021/acsami.1c05054.

[44] G. Ćirić-Marjanović, M. Trchová, J. Stejskal, The chemical oxidative polymerization of aniline in water: Raman spectroscopy, J. Raman Spectrosc. 39 (2008) 1375–1387. https://doi.org/10.1002/jrs.2007.

[45] M. Trchová, Z. Morávková, M. Bláha, J. Stejskal, Raman spectroscopy of polyaniline and oligoaniline thin films, Electrochimica Acta. 122 (2014) 28–38. https://doi.org/10.1016/j.electacta.2013.10.133.

[46] Z. Morávková, P. Bober, Writing in a Polyaniline Film with Laser Beam and Stability of the Record: A Raman Spectroscopy Study, International Journal of Polymer Science. 2018 (2018) 1–8. https://doi.org/10.1155/2018/1797216.

[47] M. Bláha, J. Zedník, J. Vohlídal, Self-doping of polyaniline prepared with the $FeCl_3/H_2O_2$ system and the origin of the Raman band of emeraldine salt at around 1375 cm^{-1}: Self-doping of polyaniline, Polym. Int. 64 (2015) 1801–1807. https://doi.org/10.1002/pi.4983.

[48] A. Hugot-Le Goff, M.C. Bernard, Protonation and oxidation processes in polyaniline thin films studied by optical multichannel analysis and in situ Raman spectroscopy, Synthetic Metals. 60 (1993) 115–131. https://doi.org/10.1016/0379-6779(93)91230-Y.

[49] R.V. Salvatierra, M.M. Oliveira, A.J.G. Zarbin, One-Pot Synthesis and Processing of Transparent, Conducting, and Freestanding Carbon Nanotubes/Polyaniline Composite Films, Chem. Mater. 22 (2010) 5222–5234. https://doi.org/10.1021/cm1012153.

[50] V.S. Jamadade, D.S. Dhawale, C.D. Lokhande, Studies on electrosynthesized leucoemeraldine, emeraldine and pernigraniline forms of polyaniline films and their supercapacitive behavior, Synthetic Metals. 160 (2010) 955–960. https://doi.org/10.1016/j.synthmet.2010.02.007.

[51] J. Zeng, H.J. Yao, S.X. Zhang, P.F. Zhai, J.L. Duan, Y.M. Sun, G.P. Li, J. Liu, Swift heavy ions induced irradiation effects in monolayer graphene and highly oriented pyrolytic graphite, Nuclear Instruments and Methods in Physics Research Section B: Beam Interactions with Materials and Atoms. 330 (2014) 18–23. https://doi.org/10.1016/j.nimb.2014.03.019.

[52] J. Zeng, J. Liu, S.-X. Zhang, P.-F. Zhai, H.-J. Yao, J.-L. Duan, H. Guo, M.-D. Hou, Y.-M. Sun, Irradiation effects of graphene and thin layer graphite induced by swift heavy ions, Chinese Phys. B. 24 (2015) 086103. https://doi.org/10.1088/1674-1056/24/8/086103.

[53] Ph. Colomban, S. Folch, A. Gruger, Vibrational Study of Short-Range Order and Structure of Polyaniline Bases and Salts, Macromolecules. 32 (1999) 3080–3092. https://doi.org/10.1021/ma981018l.

[54] D.R. Tallant, T.A. Friedmann, N.A. Missert, M.P. Siegal, J.P. Sullivan, Raman Spectroscopy of Amorphous Carbon, MRS Proc. 498 (1997) 37. https://doi.org/10.1557/PROC-498-37.

[55] A.C. Ferrari, J. Robertson, Interpretation of Raman spectra of disordered and amorphous carbon, Phys. Rev. B. 61 (2000) 14095–14107. https://doi.org/10.1103/PhysRevB.61.14095.

[56] X. Wang, L. Zhang, Green and facile production of high-quality graphene from graphite by the combination of hydroxyl radicals and electrical exfoliation in different electrolyte systems, RSC Adv. 9 (2019) 3693–3703. https://doi.org/10.1039/C8RA09752F.

[57] C.N.R. Rao, K. Biswas, K.S. Subrahmanyam, A. Govindaraj, Graphene, the new nanocarbon, J. Mater. Chem. 19 (2009) 2457. https://doi.org/10.1039/b815239j.

[58] W. Ouyang, D. Zeng, X. Yu, F. Xie, W. Zhang, J. Chen, J. Yan, F. Xie, L. Wang, H. Meng, D. Yuan, Exploring the active sites of nitrogen-doped graphene as catalysts for the oxygen reduction reaction, International Journal of Hydrogen Energy. 39 (2014) 15996–16005. https://doi.org/10.1016/j.ijhydene.2014.01.045.

[59] S.H. Huh, X-ray diffraction of multi-layer graphenes: Instant measurement and determination of the number of layers, Carbon. 78 (2014) 617–621. https://doi.org/10.1016/j.carbon.2014.07.034.

[60] A. Pandey, S. Dalal, S. Dutta, A. Dixit, Structural characterization of polycrystalline thin films by X-ray diffraction techniques, J Mater Sci: Mater Electron. 32 (2021) 1341–1368. https://doi.org/10.1007/s10854-020-04998-w.

[61] E.A. Sanches, S.M. de Souza, A.P.L. Carvalho, G. Trovati, E.G.R. Fernandes, Y.P. Mascarenhas, Nanocomposite based on polyaniline emeraldine-base and α-Al_2O_3 : A structural characterization, International Journal of Materials Research. 106 (2015) 1094–1100. https://doi.org/10.3139/146.111280.

[62] S. Bharti, J. Jacob, A.K. Ghosh, Polyaniline doped with α, ω-alkanedisulfonic acids: preparation and characterization: Alkanedisulfonic acid-doped polyaniline, Polym. Int. 62 (2013) 797–803. https://doi.org/10.1002/pi.4365.

[63] D.T. Seshadri, N.V. Bhat, Structural and electrical properties of crystals of substituted polyaniline, J. Polym. Sci. B Polym. Phys. 45 (2007) 1127–1137. https://doi.org/10.1002/polb.21158.

[64] V. Suendo, Y. Lau, F. Hidayat, M. Reza, A. Qadafi, A. Rochliadi, Effect of face-to-face and side-to-side interchain interactions on the electron transport in emeraldine salt polyaniline, Phys. Chem. Chem. Phys. 23 (2021) 7190–7199. https://doi.org/10.1039/D0CP06194H.

[65] S.J. Varma, F. Xavier, S. Varghese, S. Jayalekshmi, Synthesis and studies of exceptionally crystalline polyaniline thin films, Polym. Int. 61 (2012) 743–748. https://doi.org/10.1002/pi.4131.

[66] J. Gao, J. Huang, Z. Huang, Q. Meng, L. Zheng, Q. Sun, G. Li, Catalytic growth of highly crystalline polyaniline by copper under ambient conditions, CrystEngComm. 20 (2018) 5119–5122. https://doi.org/10.1039/C8CE00893K.

[67] R.C. Ramola, S. Chandra, J.M.S. Rana, R. Sharma, S. Annapoorni, R.G. Sonkawade, D.K. Avasthi, Swift heavy ions induced modifications in structural and electrical properties of polyaniline, Current Science. 97 (2009) 1453–1458.

[68] A.R. Stokes, A.J.C. Wilson, A method of calculating the integral breadths of Debye-Scherrer lines: generalization to non-cubic crystals, Math. Proc. Camb. Phil. Soc. 40 (1944) 197–198. https://doi.org/10.1017/S0305004100018314.

[69] D. Fink, W.H. Chung, R. Klett, A. Schmoldt, J. Cardoso, R. Montiel, M.H. Vazquez, L. Wang, F. Hosoi, H. Omichi, P. Goppelt-Langer, Carbonaceous clusters in irradiated polymers as revealed by UV-Vis spectrometry, Radiation Effects and Defects in Solids. 133 (1995) 193–208. https://doi.org/10.1080/10420159508223990.

[70] W.S. Huang, A.G. MacDiarmid, Optical properties of polyaniline, Polymer. 34 (1993) 1833–1845. https://doi.org/10.1016/0032-3861(93)90424-9.

[71] S. Stafström, J.L. Brédas, A.J. Epstein, H.S. Woo, D.B. Tanner, W.S. Huang, A.G. MacDiarmid, Polaron lattice in highly conducting polyaniline: Theoretical and optical studies, Phys. Rev. Lett. 59 (1987) 1464–1467. https://doi.org/10.1103/PhysRevLett.59.1464.

[72] M. Abdolkarimi-Mahabadi, A. Bayat, A. Mohammadi, Use of UV-Vis Spectrophotometry for Characterization of Carbon Nanostructures: a Review, Theor Exp Chem. 57 (2021) 191–198. https://doi.org/10.1007/s11237-021-09687-1.

[73] J. Tauc, R. Grigorovici, A. Vancu, Optical Properties and Electronic Structure of Amorphous Germanium, phys. stat. sol. (b). 15 (1966) 627–637. https://doi.org/10.1002/pssb.19660150224.

[74] M.M. Abutalib, Insights into the structural, optical, thermal, dielectric, and electrical properties of PMMA/PANI loaded with graphene oxide nanoparticles, Physica B: Condensed Matter. 552 (2019) 19–29. https://doi.org/10.1016/j.physb.2018.09.034.

[75] R. Kumar, S. Asad Ali, A.H. Naqvi, H.S. Virk, U. De, D.K. Avasthi, R. Prasad, Study of optical band gap and carbon cluster sizes formed in 100 MeV Si8+ and 145 MeV Ne6+ ions irradiated polypropylene polymer, Indian J Phys. 83 (2009) 969–976. https://doi.org/10.1007/s12648-009-0056-5.

[76] J. Robertson, E.P. O'Reilly, Electronic and atomic structure of amorphous carbon, Phys. Rev. B. 35 (1987) 2946–2957. https://doi.org/10.1103/PhysRevB.35.2946.